JOURNAL OF GEOPHYSICAL RESEARCH, VOL. 104, NO. D3, PAGES 3655-3667, FEBRUARY 20, 1999

An evaluation of chemistry's role in the winter-spring ozone maximum found in the northern midlatitude free troposphere

J. J. Yienger,[1] A. A. Klonecki,[2] H. Levy II,[3] W. J. Moxim,[3] and G. R. Carmichael[1]

Abstract. We employ the Geophysical Fluid Dynamics Laboratory global chemical transport model to investigate the contribution of photochemistry to the winter-spring ozone maximum in the northern hemisphere (NH) midlatitude free troposphere (770-240 mbar; 30°N-60°N). Free tropospheric ozone mass slowly builds up in the winter and early spring, with net chemistry and transport playing comparable roles. Winter and early spring conditions are favorable to net ozone production for two reasons: (1) Winter conditions (cold, low Sun angle, and dry) reduce HO_x and lower the level of NO_x needed for chemical production to exceed destruction (balance point); and (2) throughout the winter and early spring, NO_x, because of its longer chemical lifetime, increases above normally net-destructive levels in the remote atmosphere. Interestingly, net production in the midlatitude NH free troposphere maximizes in early spring because relatively high NO_x and low balance point conditions are present at a time when increasing insolation is speeding up photochemistry. Conceptually, the net ozone production is associated with an annual atmospheric "spring cleaning" in which high levels of NO_x are removed via OH oxidation. Further, we find that human activity has a major impact on both the levels of tropospheric ozone and the role of chemistry in the NH midlatitude, where anthropogenic NO_x emissions dominate. In that region, modern ozone levels have increased by ~20% in the winter and ~45% in the spring, winter-spring chemistry has switched from net destructive to net productive, the winter-spring balance between transport and chemistry has switched from transport dominance in preindustrial times to the present parity, and the preindustrial February maximum has progressed to March-April. Estimated 2020 levels of NO_x emissions were found to lead to even greater net production and to push the O_3 spring maximum later into April-May.

1. Introduction

The seasonal cycle of tropospheric ozone continues to be a topic of considerable interest in atmospheric chemistry. At surface stations in the remote northern hemisphere (NH), ozone distinctly maximizes in the spring [*Oltmans,* 1981; *Oltmans and Levy,* 1994], and it has been argued that this is largely a result of a springtime injection of stratospheric ozone [e.g., *Levy et al.,* 1985; *Oltmans and Levy,* 1992; *Moody et al.,* 1995]. In the polluted continental boundary layer, the rise of ozone in spring continues into summer because of very strong in situ pollution-mediated ozone production [e.g., *Logan,* 1985]. In the free troposphere, however, the seasonal cycle is not as extensively observed, and no comprehensive analysis has been performed. Long-term ozonesonde measurements from a limited number of remote sites [e.g., *Oltmans et al.,* 1996] clearly show a spring maximum, while the large majority of ozonesondes are launched from the polluted continental boundary layer and experience a spring-summer ozone maximum up to 500 mbar [*Logan,* 1985]. It has been inferred that the former supports a major role for transport from the stratosphere and that the latter points to a major role for chemical production [*Levy et al.,* 1985; *Logan,* 1985]. Chemical explanations for a springtime ozone maximum based on chemical lifetimes and ozone production efficiency have also been advanced [e.g., *Penkett and Brice,* 1986; *Liu et al.,* 1987; *Lin and Liu,* 1988]. These observations, inferences, and analyses, for both the boundary layer and the free troposphere, have fueled an ongoing debate over "stratospheric injection versus tropospheric chemistry" [e.g., *Levy et al.,* 1985; *Logan,* 1985; *Liu et al.,* 1987; *Follows and Austin,* 1992; *Jacob et al.,* 1993; *Parrish et al.,* 1993; *Muller and Brasseur,* 1995]. Several recent global chemical transport model (GCTM) studies provide evidence that both mechanisms are important [*Levy et al.,* 1997; *Roelofs and Lelieveld,* 1997; *Bernsten and Isaksen,* 1997].

The ability of recent GCTM simulations to capture major observed features of tropospheric ozone suggests that we now have an appropriate tool for a comprehensive analysis of the nature and extent of the springtime ozone maximum in the free troposphere. For this study we analyze a zonal volume (30°N-60°N) containing the model's free troposphere (770-240 mbar). This region, the NH midlatitude free troposphere, contains much of the world's pollution, as well as large areas

[1]Center for Global and Regional Environmental Research, University of Iowa, Iowa City.
[2]Atmospheric Oceanic Sciences Program, Princeton University, Princeton, New Jersey.
[3]NOAA Geophysical Fluid Dynamics Laboratory, Princeton, New Jersey.

Paper Number 1998JD100043.
0148-0227/99/1998JD100043$09.00

of the background troposphere, and is also strongly influenced by stratosphere-troposphere exchange. By including the full zonal volume in our study, we exclude complex regional transport issues and focus on very large scale features of both transport and chemistry. In section 2 we briefly describe the GCTM used in the study and discuss the simulated winter-spring maximum. In section 3 we extend the work of *Klonecki and Levy* [1997] to examine and quantify the chemical basis for a springtime ozone maximum. We then construct the zonal budgets and quantify the relative contributions of both large-scale transport and in situ chemistry. Last, after discussing the impact of human activity on the budgets and the role of chemistry, we examine sources of uncertainty in this analysis and summarize our conclusions.

2. Ozone Simulation

The Geophysical Fluid Dynamics Laboratory (GFDL) global chemical transport model (GCTM) has a horizontal resolution of ~265 km, has 11 sigma levels in the vertical at standard pressures of 10, 38, 65, 110, 190, 315, 500, 685, 835, 940, and 990 mbar, and is driven by 12 months of 6-hour time-averaged winds, temperatures, and precipitation fields from a general circulation model. The transport portion of the GCTM employees a numerical scheme which is second order in the horizontal and fourth order in the vertical for resolved (grid-scale) advection [see *Mahlman and Moxim,* 1978, section 3] and includes diffusion-based parameterizations for horizontal subgrid-scale transport and for vertical subgrid-scale transport due to dry and moist convection throughout the troposphere and shear-dependent mixing in the boundary layer [see *Levy et al.*,1985; *Kasibhatla et al.*, 1996, and references therein]. For our analysis, three model levels (315, 500, and 685 mbar) comprise the free troposphere (770-240 mbar), and the three lowest model levels (835, 940, and 990 mbar) form the boundary layer (surface to 770 mbar).

The ozone simulation has four components: irreversible stratospheric injection, CH_4-CO-H_2O-NO_x based chemistry throughout the background troposphere, parameterized pollution production in the continental boundary layer (BL), and surface dry deposition [see *Levy et al.*, 1997; *Klonecki and Levy,* 1997].

The model's explicitly simulated stratospheric injection has been significantly improved over previous efforts [*Levy et al.,* 1997] by relaxing, with a 10-day lifetime, the GCTM's lower stratospheric ozone values to those simulated by the GFDL SKYHI GCM [*Hamilton et al.,* 1995; L. Perliski, private communication, 1997]. The SKYHI GCM, with greatly improved resolution in the stratosphere, produces a more quantitatively realistic simulation of lower stratospheric ozone (L. Perliski, private communication, 1997) than does the GCTM [*Mahlman et al.*, 1980; *Levy et al.*, 1985]. While this relaxation significantly improves the GCTM's simulation of upper tropospheric ozone in the extratropics of both hemispheres, it does introduce a potential transport ambiguity in the lower stratosphere, where we expect the GCTM and the SKYHI GCM to have different meteorologies. As a compromise, which appears to be effective, we relax, rather than instantaneously restore, the lower stratospheric GCTM ozone values to the monthly-mean zonally averaged SKYHI GCM ozone values, rather than to local instantaneous SKYHI values. The resulting global net stratospheric injection of ozone into the troposphere decreases from the previous value of 696 Tg O_3/yr to 629 Tg O_3/yr.

A CH_4-CO-H_2O-NO_x photochemical box model is used to construct seven-parameter interpolation tables for 24-hour averaged rates of ozone production and destruction in the background troposphere (NO_x < 200 parts per trillion by volume (pptv); isoprene < 100 pptv). With CH_4 being specified for each hemisphere, the seven parameters are tropospheric pressure, latitude, month, albedo, O_3, NO_x, CO, and H_2O. The tables are constructed for the GCTM tropospheric pressure levels, 17 latitude bands, every other month, both land and sea albedos, and for a range of O_3, NO_x, CO, and H_2O mixing ratios corresponding to values observed in the troposphere [see *Klonecki and Levy,* 1997]. In these photochemical calculations, H_2CO, H_2O_2, and CH_3O_2H are assumed to be in photochemical diurnal steady state, HNO_3 is specified at observed levels, and the very small direct contribution to ozone production from the peroxyacetyl radical is not considered. Ozone destruction is not sensitive to any of the steady state or specified species. While ozone production has some sensitivity to peroxide level in the extratropical upper troposphere, local photochemical steady state is generally an upper limit in that region, and recent studies have found that even an extreme 100% change in 315-mbar ozone production results in only a 10-30% change in ozone [*Klonecki,* 1998]. Uncertainties in ozone production due to the steady state assumption for the peroxides are much less than 100%.

The instantaneous ozone production and destruction terms for every grid box in the background troposphere are then interpolated every time step from the tables using (1) the instantaneous ozone concentration from the current simulation; (2) monthly averaged CO and 6-hour averaged NO_x concentrations from earlier simulations using the same meteorology; and (3) monthly averaged H_2O from observations [*Oort,* 1983; *Soden and Bretherton,* 1996]. Thus the O_3 chemical rates respond to most significant fluctuations in O_3, NO_x, and CO generated by the GCTM. While observed monthly-mean H_2O does not include all of its local fluctuations, the dominant variations with height, latitude, and season are captured.

The GCTM simulation of NO_x includes all known sources: fossil fuel combustion (23.8 Tg N/yr), biomass burning (7.7 Tg N/yr), soil-biogenic emissions (5.0 Tg N/yr), lightning discharge (3 Tg N/yr), aircraft emissions (0.45 Tg N/yr), and stratospheric injection (0.64 Tg N/yr) [see *Levy et al.*, 1996, and references therein]. Three families of tracers (nitrogen oxides, peroxyacetyl nitrate (PAN), and HNO_3) are transported, and the effective first-order rate coefficients for gas phase and heterogeneous chemical conversions among the families are precalculated off-line for specified monthly-mean zonally averaged fields of O_3, NO_x, CO, CH_4, and H_2O [see *Kasibhatla et al.,* 1993]. The inclusion of PAN is critical to the distribution of NO_x away from source regions [*Moxim et al.,* 1996]. Without our coupling of biogenic and lightning emissions to the GCTM's meteorology, we would miss the strong episodic emissions of biogenic NO_x [see *Yienger and Levy,* 1995, Figure 4], and our effective emissions from lightning, which are a major summertime source of NO_x in the region under study, would be underestimated by at least 30% and incorrectly distributed in the vertical [see *Levy et al.,* 1996].

The GCTM's HNO_3 wet deposition is well correlated to 236 observations from around the world (correlation coefficients from 0.75 to 0.87) and clearly captures the observed

global patterns of wet deposition, with 75% of the observations agreeing within ±50%. The GCTM's NO_x fields are in reasonable agreement with the large majority of the observations (~50% within ±25% and ~75% within ±50%), show no systematic global biases, display the observed vertical profiles, and have high levels (~1 ppbv or greater) in the polluted BL and very low values in the remote BL. In general, the level of agreement between simulation and observation is as good as the agreement between separate, but simultaneous, observations of NO, NO_x, or NO_y.

The GCTM simulation of CO includes sources from fossil fuel (350 Tg CO/yr), biomass burning (647 Tg CO/yr), biogenic hydrocarbon oxidation (631 Tg CO/yr), and CH_4 oxidation (664 Tg CO/yr) and employs precalculated monthly-mean zonally averaged OH fields [*Spivakovsky et al.*, 1990] for CO destruction (T. Holloway, private communication, 1998). Model results were compared with observations from the 33 NOAA Climate Monitoring and Diagnostics Laboratory global cooperative flask sampling network stations which measure CO (P. C. Novelli, private communication, 1997). Over most of the globe, there is good agreement, with 86% of seasonal averages agreeing within 25% between model and observations. For all of the outliers (18 points out of 132) the model overestimated CO concentrations, suggesting a high bias in the simulation. In the southern hemisphere, an overestimation of CO from biogenic hydrocarbons is a likely source of error.

Although the O_3 simulation is responding to most of the important fluctuations in the species important to its chemistry, the same is not necessarily true for CO and NO_x, where the monthly-mean zonally averaged chemical rates were precalculated for specified fields of O_3, NO_x, CO, and H_2O. This should not be a problem for CO, which has a chemical lifetime of months (T. Holloway, private communication, 1998) and is not that sensitive to day-to-day fluctuations in its chemical loss rate. However, NO_x, with a chemical lifetime of days, may be. When O_3 levels were varied by ±25%, NO_x levels were generally insensitive, with changes of only 5-10% [*Klonecki*, 1998]. Only for the summertime 25% ozone reduction did midlatitude NO_x change (increase) by as much as 15-20%. Considering these NO_x sensitivities along with the fact that midlatitude O_3 is not very sensitive to variations in its chemical production [*Klonecki*, 1998] and the relatively long CO chemical lifetime, we do not expect the lack of chemical feedbacks for NO_x and CO to significantly affect the conclusions of this study.

Both the parameterized net production in the polluted continental boundary layer (NO_x > 200 pptv; isoprene > 100 pptv), which is derived from an empirical relationship between NO_x conversion and O_3 production based on midlatitude observations and theoretical studies, and surface dry deposition are as described previously [*Kasibhatla et al.*, 1996; *Levy et al.*, 1997]. The direct net production of ozone in the polluted BL plays only a small role in the region of this study [*Levy et al.*, 1997].

In a recent study of human impact on tropospheric ozone [*Levy et al.*, 1997], an earlier version of the O_3 simulation was compared with ~200 seasonal observations from 21 ozonesonde sites, 12 surface sites, and the Transport and Atmospheric Chemistry Near the Equatorial Atlantic (TRACE-A) aircraft mission. We found that 73% of the comparisons agreed within ±25%, while only 10% of the cases were significant outliers. With our improvement in the simulation of irreversible injection from the stratosphere, biases in both hemispheres have been significantly reduced, and our current comparison with over 300 seasonal data points now finds that almost 90% of the cases agree within ±25%. The agreement is even better for the subset of data in the NH midlatitude free troposphere.

A more detailed assessment of the midlatitude free troposphere is provided in Figure 1, where 500-mbar monthly means are compared for representative midlatitude stations. For Hohenpeissenberg (Figure 1a) we have plotted each of the last 16 years of monthly means separately to show the midlatitude interannual variability, which our GCTM cannot simulate with only 1 year of model meteorology. In all years, there is a general pattern of a winter minimum and a spring-summer maximum, though the actual maximum varies from year to year. Our simulation captures this general behavior, though January is high and May is low. In Figures 1b-1d the simulated monthly means are compared with multiple-year averages of observed monthly means. Although the observations and simulations have the same general pattern of a winter minimum and a spring-summer maximum and their monthly standard deviations strongly overlap, there are systematic differences between the one model year and the observed climatologies. The simulated late winter generally exceeds observations, and the simulated August maximum is generally, though not always (see Figure 1a), later than the observed maximum. While still far from perfect, this GCTM simulation appears to provide a realistic picture of ozone's distribution in the troposphere and should be an appropriate tool for analyzing and quantifying the role of chemical production in the winter-spring maximum of tropospheric ozone.

In Figure 2 we present a monthly-mean time series of the total mass of O_3 simulated for the NH midlatitude free troposphere. The prominent features of this time series are a clear spring maximum, which has already been observed in radioactive debris [e.g., *Mahlman*, 1969; *Mahlman and Moxim*, 1978], a gradual summertime decrease, and a minimum in the late fall, all of which are consistent with observed behavior away from the polluted continental BL [e.g., *Oltmans et al.*, 1996]. The slight resurgence of late summer O_3 mass seen in Figure 2 is consistent with the summer maximum observed in the free troposphere over polluted regions (see Figure 2 and *Logan* [1985]). In section 3 we examine the theory behind the role of chemistry in the winter-spring maximum shown in Figure 2 and explore its dependence on month, latitude, and altitude.

3. CO/CH_4 Ozone Production in the Winter and Spring

While ozone photochemistry slows greatly in the winter [e.g., *Levy et al.*, 1985; *Klonecki and Levy*, 1997], the net chemical tendency becomes positive throughout the free troposphere of the northern midlatitudes (see Figure 3, in which net chemical tendency for the 30°N-60°N free tropospheric control volume is separated into production and destruction). From June through September, free tropospheric chemistry is very active, but, when averaged over the control volume, it is nearly in balance. In surprising contrast, the much slower winter-spring chemistry is net productive from late fall through the winter and reaches a maximum in the early

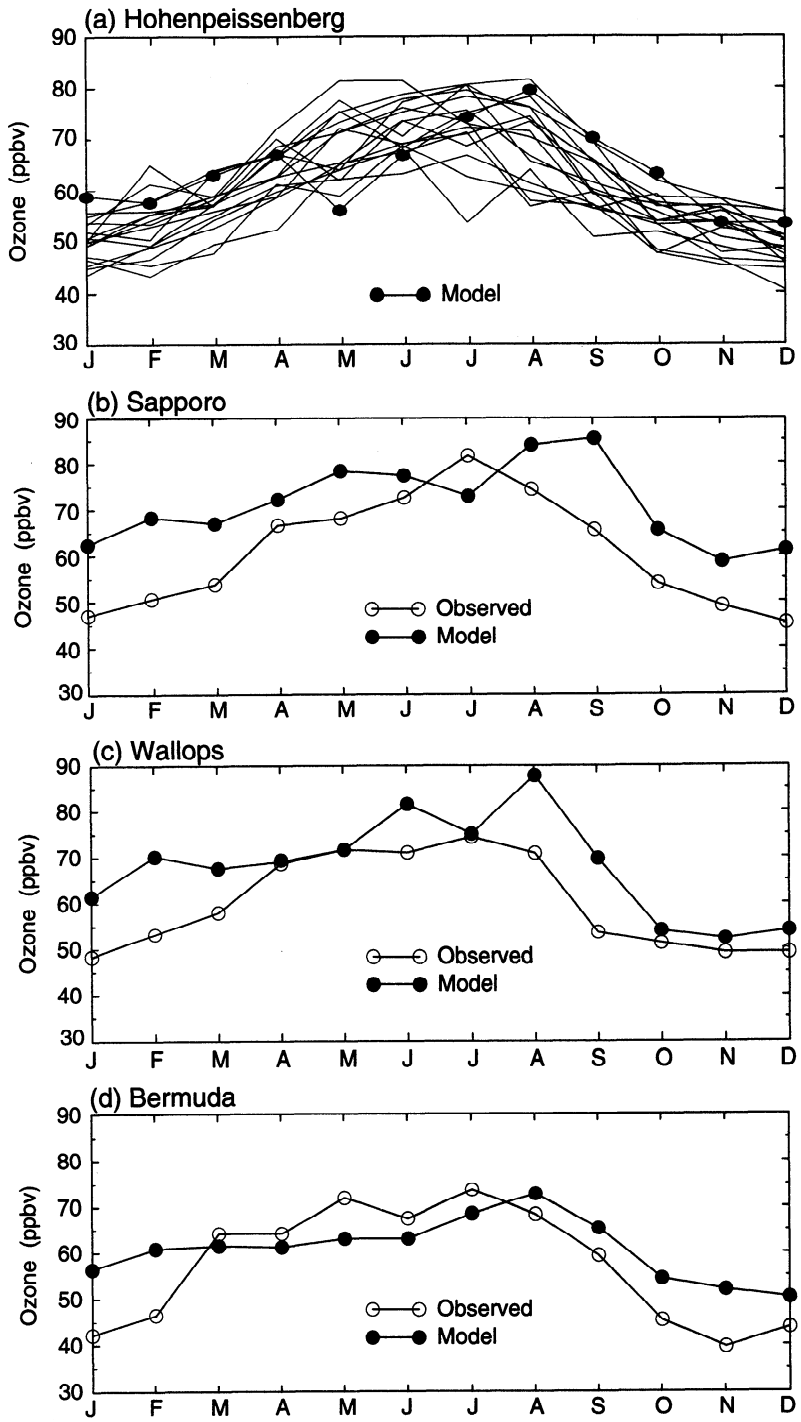

Figure 1. Seasonal plots of observed and simulated (solid circles) monthly-mean 500 mbar O_3 mixing ratios (ppbv): (a) Hohenpeissenberg, with observed individual years denoted as straight lines; (b) Sapporo, Japan, with observed monthly means averaged over all years denoted as the open circles; (c) Wallops, Virginia, with the observed monthly means averaged over all years denoted as the open circles; and (d) Bermuda, with the observed monthly means averaged over all years denoted as the open circles and April set equal to March.

spring. In order to understand this intriguing counterintuitive behavior, we must first examine the chemical mechanism.

Ozone destruction is initiated through

(R1) $O_3 + h\nu \rightarrow O_2 + O(^1D)$

(R2) $O(^1D) + H_2O \rightarrow 2OH$

Further direct destruction occurs through

(R3) $O_3 + OH \rightarrow O_2 + HO_2$

(R4) $O_3 + HO_2 \rightarrow 2O_2 + OH$

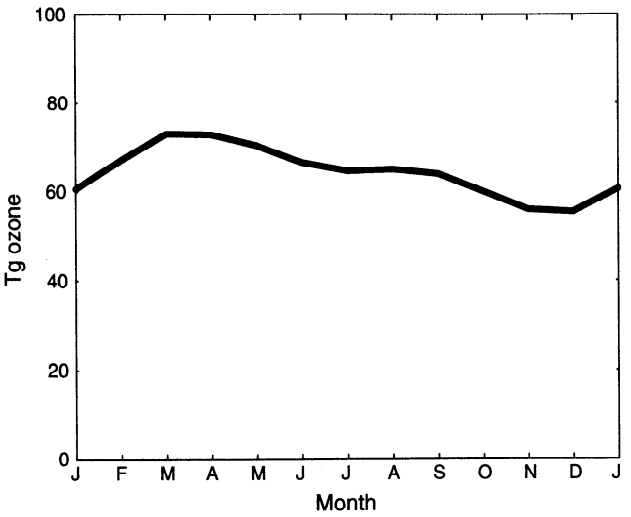

Figure 2. Annual time series of monthly-mean simulated ozone mass (teragrams) for the free troposphere (~2-10 km) between 30°N and 60°N.

Ozone production requires NO_x

(R5) $NO + HO_2 \rightarrow NO_2 + OH$

(R6) $NO + CH_3O_2 \rightarrow NO_2 + CH_3O$

(R7) $NO_2 + h\nu \rightarrow NO + O(^3P)$

(R8) $O(^3P) + O_2 + M \rightarrow O_3 + M$

"Ozone chemical tendency" is calculated as the difference between gross production, which can be approximated as the sum of the rate-determining reactions, (R5) and (R6), and gross destruction, the sum of (R2), (R3), and (R4). The seasonality of the chemical tendency varies dramatically with altitude (see Figure 4). Year-round net production in most of the upper troposphere [see *Klonecki and Levy*, 1997] stands out clearly in Figure 4a. The 500-mbar level in Figure 4b is slightly destructive in the summer and slightly productive in the winter-spring, while the 685-mbar level in Figure 4c is destructive in the summer and productive in winter-spring. The summertime net destruction of the lower two levels is almost canceled by the net production of the upper troposphere, while all three levels contribute to net chemical production in winter-spring.

One of the most interesting features of Figure 4 is the switch from net destruction in the summer to production in the winter and spring below 500 mbar. Recently, *Klonecki and Levy* [1997] showed that for a given level of ozone, the lower humidities, temperatures, and zenith angles of wintertime all reduce the amount of NO_x needed for gross ozone production to equal gross destruction (defined as the "balance point"). In winter (R1) is reduced considerably. Reaction (R2) is additionally slowed by lower H_2O, and the rates of (R3) and (R4) are also reduced by lower mixing ratios of HO_x radicals. For NO_x near the balance point, production also decreases (fewer HO_2 and CH_3O_2 radicals) but by less than destruction. Consequently, it takes less NO_x in winter than in summer to balance ozone production and destruction.

Wintertime net production is amplified below 500 mbar by our simulated increase in midlatitude NO_x during winter (see Figure 5). In the July, high NO_x levels occur mainly above source regions, where convective transport is active. Rapid photochemical loss of the NO_x and relatively slow transport prevent its spread far beyond source regions. In January, although convection is weaker, winter storms lift surface NO_x into the free troposphere, where stronger westerlies and weaker chemical loss allow it to spread widely. The high NO_x levels over the remote oceans, to which the decomposition of transported PAN is an important contribution [*Moxim et al.*, 1996], do not begin to disappear until April and May (figure not shown).

We now focus on the model's 685-mbar level (lower free troposphere), which drives the seasonal behavior shown in Figure 3. As a result of the decreasing balance point and increased level of NO_x, most of the level switches to net chemical production in winter and early spring. In Figure 6 we show the chemical tendency's evolution at 685 mbar from winter through spring. From January to March, net production is a maximum over and just downwind of major source regions, and a belt of net production extends around the globe, driven by both a lower balance point and elevated NO_x levels. North of 60°N, chemistry is so slow that the net tendency is essentially zero regardless of NO_x concentration. By April, because of the shift of the balance point to higher NO_x and the rapid depletion of the high NO_x in remote regions, the average net chemistry becomes destructive over the oceans south of 60°N, though production continues over source regions. North of 60°N, processing of high spring NO_x is now "turned on", as is net ozone production. While wintertime net production occurs over 80% of the region, by June the NH shows net destruction over 85% of the region and net production is only found near the polluted continents (15%).

Our calculated chemical tendencies compare well with a number of analyses based on data from regional field experiments [e.g., *Chameides et al.*, 1992; *Crawford et al.*, 1997; *Klonecki and Levy*, 1997; *Penkett et al.*, 1998]. Analysis of observations from the Pacific Exploratory Mission (PEM-West B) Campaign [*Crawford et al.*, 1997], found net photochemical ozone production in the free troposphere and marine BL out to 2000 km offshore of Asia during spring. Our simu-

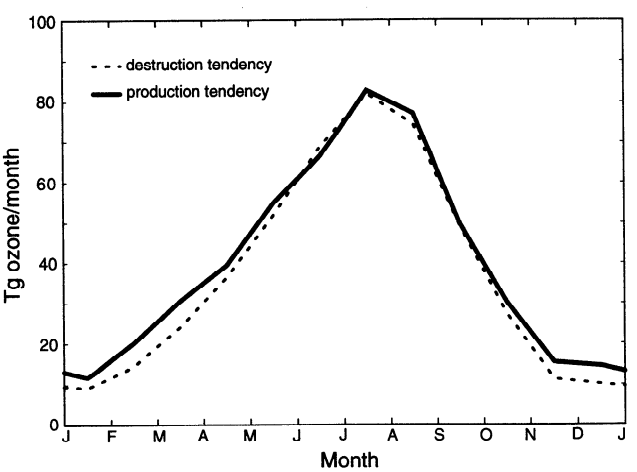

Figure 3. Annual time series of monthly-mean simulated chemical production and destruction (Tg/month) between 30°N and 60°N for the free troposphere (~2-10 km).

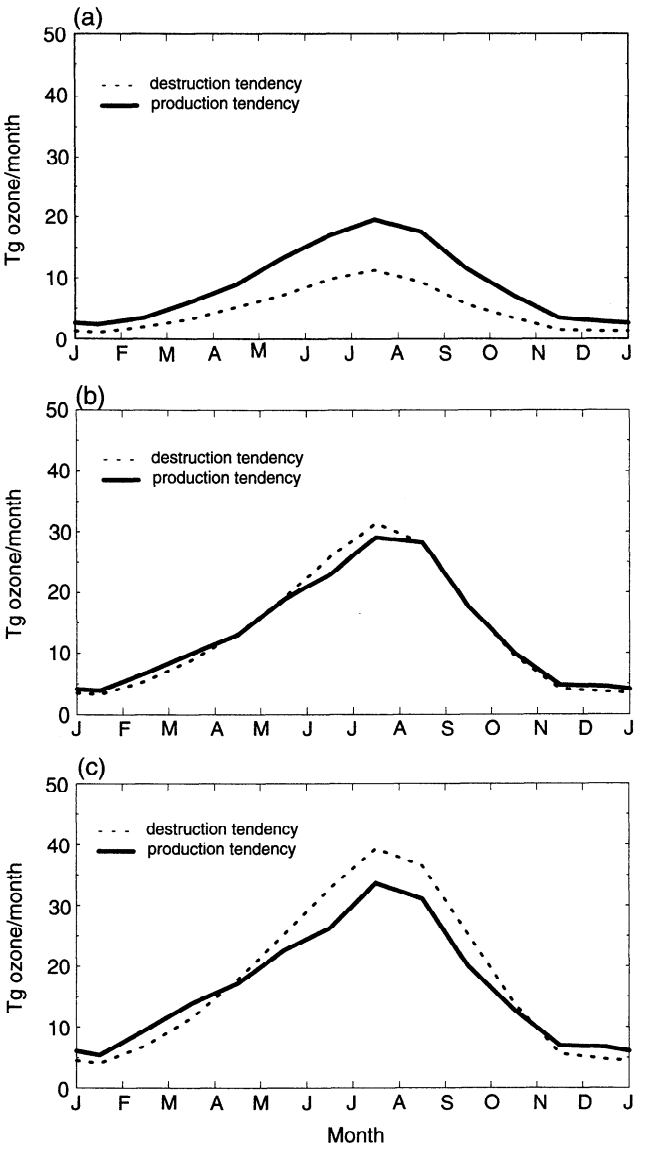

Figure 4. Annual time series of ozone production and destruction (Tg/month) between 30°N and 60°N for individual levels: (a) 315 mbar, (b) 500 mbar, and (c) 685 mbar. The sum of all three equals the net chemical tendency curve shown in Figure 9b.

lated net production rate in the same area (south of Japan and east of China) of 40-60 ppb/month is similar to observed column production rates of 1-3% per day. Observed decreases in critical NO (equivalent to our NO_x balance point) with increasing latitude and altitude [*Crawford et al.*, 1997] are consistent with the theoretical analyses of *Klonecki and Levy* [1997] and our global simulation. In the eastern North Atlantic, *Penkett et al.* [1998] infer significant springtime ozone production from calculated and measured peroxide data. Our model, which finds net production over much of the North Atlantic during spring, is consistent with this inference.

In Figure 7, we present the simulated time series of zonally averaged net chemical tendency at 685 mbar, broken into 10° intervals between 30°N and 70°N. At all latitudes, there is a distinct spring net production maximum of ~10 ppbv/month, followed by a rapid switch to net destruction. Since the notion of "spring" depends on latitude, the timing of the maximum occurs later at higher latitudes. Referring back to Figure 6, we see that zones of net chemical destruction do indeed progress northward from February-March in midlatitudes to May in high latitudes. The spring production maximum at each latitude results from a brief period of enhanced NO_x catalyzed ozone production, which is accompanied by dry spring air that moderates the increase in destruction. As water vapor concentration and insolation increase, NO_x is rapidly depleted by enhanced OH, and the atmosphere reverts to net destruction. In Figure 8, the relationships among the phases for the time series of zonally averaged monthly-mean NO_x, H_2O, net ozone tendency, and insolation are most clearly displayed in the high-latitude band (60°N-70°N), where there is no direct interference from strong local NO_x sources. Winter conditions virtually shut off photochemistry and NO_x levels increase to ~60 pptv by January. High NO_x and dry conditions persist up to spring, when chemistry begins to accelerate. Between April and May, NO_x falls by 20 pptv but is still high enough to generate a burst of springtime net production. By June the high-latitude band, along with the rest of the 685-mbar level, is in net chemical destruction.

Water vapor [*Oort*, 1983], which is directly coupled to temperature, lags insolation by approximately 1 month (see Figure 8) due to thermal inertia (B. Soden, private communication, 1997). This lag keeps the spring atmosphere dry and slows both ozone destruction and NO_x loss. Correspondingly, early fall conditions are too moist and too NO_x deprived to support net production. This natural lag has implications not only for ozone chemistry but also for the seasonality of nearly all reactive chemistry, because the interaction of insolation and water vapor controls the oxidizing capacity of the troposphere through (R1) and (R2) [*Levy*, 1971].

4. 30°-60°N Free Tropospheric Seasonal Ozone Budget

In the free troposphere, seasonal-scale fluctuations of ozone mass in a grid box or region are a result of net imbalances in transport tendency (inward versus outward advection and diffusion) and/or chemical tendency (photochemical production versus destruction). We account for these terms by applying mass conservation over the volume of interest and using Reynold's transport equation. This can be represented symbolically by

$$\frac{\partial}{\partial t}\iiint_V \rho\, dV = -\iint_A (\rho\vec{V} + \vec{F}) \cdot dA + \text{sources} - \text{sinks} \qquad (1)$$

where the triple integral represents the time rate of change of O_3 mass inside the volume, the double integral represents the large-scale ($\rho\vec{V}$) and subgrid-scale ($\vec{F}$) mass fluxes across the volume's boundary, respectively, and the source and sink terms represent the in situ chemical production and destruction and deposition rates.

In this analysis we apply a specific form of equation (1) appropriate to our GCTM and integrate it over a month for the full zonal volume under study (770-240 mbar; 30°N-60°N). With the free troposphere having no deposition sink for ozone, this integration gives

$$\Delta O_3 = (\text{large-scale convergence} + \text{diffusive flux convergence}) + (\text{chemical production} - \text{chemical destruction}) = (\text{transport tendency}) + (\text{chemical tendency}) \qquad (2)$$

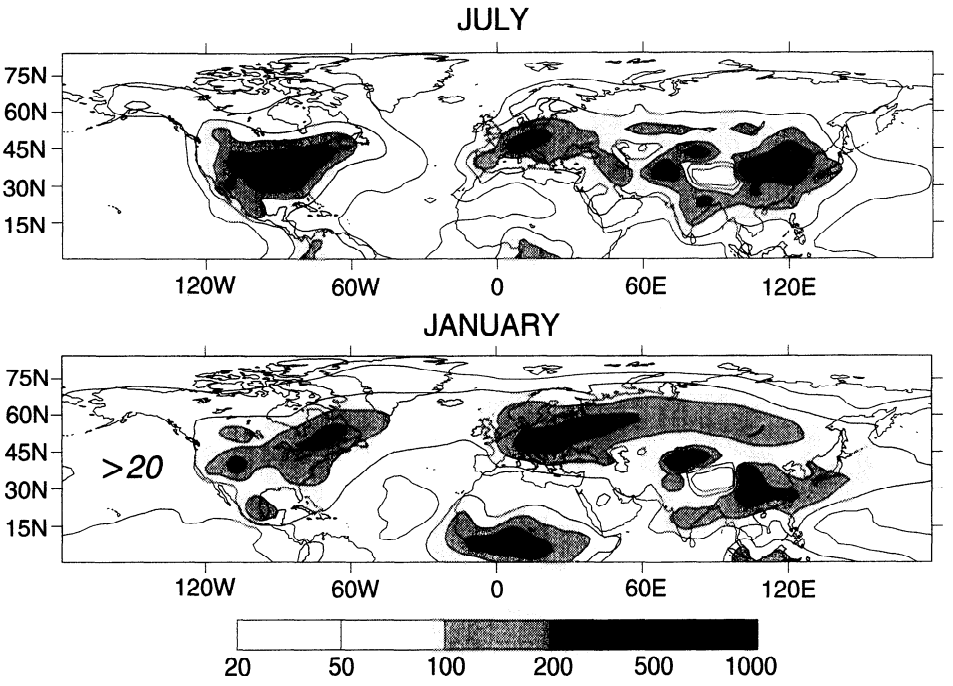

Figure 5. Simulated NO_x mixing ratios (pptv) for the 685-mbar level (~2-4 km) for January and July.

where all terms have units of Tg O_3/month. ΔO_3 is simply the monthly change in mass inside the zonal volume. The transport terms represent the net ozone convergence or divergence in the zonal volume due to large-scale advection and subgrid-scale diffusion summed over a month. The chemical terms represent monthly sums of ozone destruction and production in the zonal volume under study. Equation (2) is a simple but powerful tool for assessing the relative importance of transport and chemistry in the northern midlatitude free troposphere.

The monthly integrals of the transport and chemistry tendencies for the full zonal volume are shown in Figure 9. Winter is the only time that zonal net transport and chemistry are both positive; hence the simulated spring maximum results from both net transport and net in situ chemical production. We find that of the 18-Tg mass buildup in winter (December-February), 7 Tg (40%) is due to net transport and 11 Tg (60%) is due to net chemistry. Net production indeed maximizes in the spring while transport becomes strongly negative (i.e., out of the free troposphere), and the total volume mass of O_3 then starts to decrease, as was shown in Figure 2. Throughout the summer, transport and chemistry are essentially in balance, and there is little change in the total volume mass of O_3. After a final dip in the fall due primarily to net transport out of the volume, the winter increase begins anew, with both net transport and chemistry again becoming positive.

5. Human Impact

Because widespread winter-spring ozone production is particularly dependent upon elevated NO_x levels and anthropogenic processes dominate winter-spring NO_x emissions, it is important to characterize the present and future impact of human activity on the seasonal balance of ozone photochemistry and on the relative roles of chemistry and transport. We estimate this impact with two additional O_3 simulations that employ preindustrial and projected year 2020 NO_x levels and present levels of CO and CH_4. The OH fields were unchanged for the NO_x simulations. While this treatment is an approximation of the overall human impact on O_3, we argue that it captures the first-order impact of present and future human activity.

NO_x is the dominant factor in O_3 chemistry and much more important than CO and CH_4 [*Klonecki and Levy*, 1997]. Any OH changes from preindustrial through 2020 have only second-order effects on the NO_x simulations in comparison with the changes in NO_x emissions [see *Galloway et al.*, 1994, and references therein]. Note that the HO_x chemistry is not fixed in the O_3 simulation, only in the CO and NO_x simulations. Since 2020 CO is estimated to only increase by ~15% from present levels (T. Holloway, private communication, 1998), it should have no significant impact on the O_3 simulation [*Klonecki and Levy*, 1997], and while preindustrial CO and CH_4 are only ~40% of present (T. Holloway, private communication, 1998), preindustrial ozone chemistry is dominated by destruction, which is not sensitive to either [*Levy et al.*, 1997; *Klonecki and Levy*, 1997].

The preindustrial NO_x source (7 Tg N/yr) excludes fossil fuel emissions and fertilizer induced biogenic emissions and reduces biomass burning by a factor of 10 [see *Kasibhatla et al.*, 1996, Appendix]. The estimated 2020 NO_x source assumed no improvements in emission controls or energy efficiency, continued rapid economic development in Asia [*van Aardenne et al.*, 1998], and scaled present combustion emissions outside of Asia to the year 2020 projected regional energy use [*Energy Information Administration*, 1996]. While this can be considered an "upper limit NO_x emission scenario" for 2020, it employs a detailed analysis of economic growth, energy needs, and fuel consumption in Asia, where 60% of the increased NO_x emission is predicted

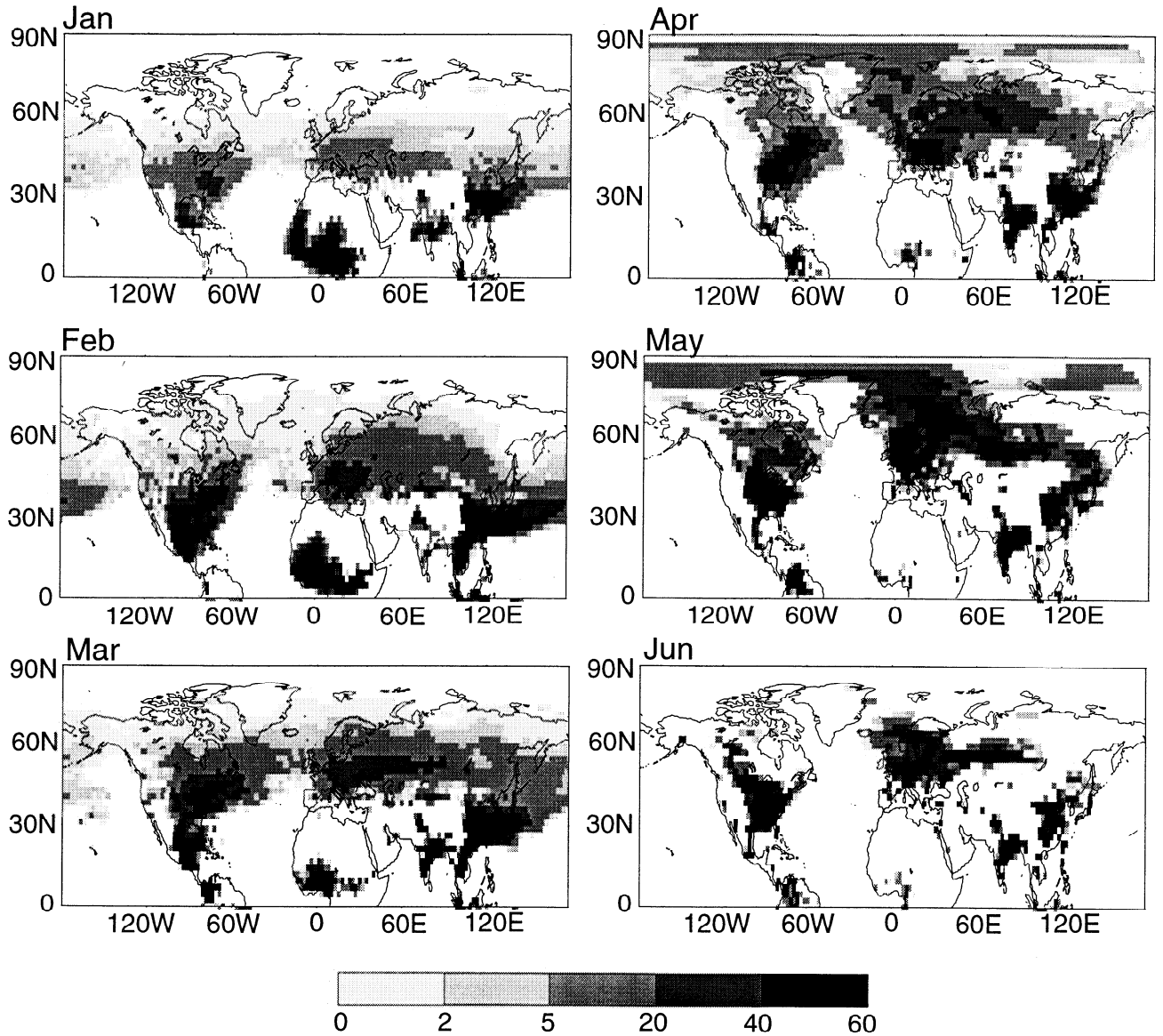

Figure 6. Monthly (January through June) variation of northern hemisphere ozone photochemical tendency (ppbv O_3/month) for the 685-mbar level (~2-4 km). Grey shadings indicate levels of net photochemical ozone production, and white indicates neutral or net destruction.

[*van Aardenne et al.*, 1998], and is relatively conservative for the rest of the industrial world. Moreover, the exact level of 2020 NO_x is not critical to our conclusions, since they are extremely robust to increased NO_x. The total NO_x source strengths are 7, 38, and 79 Tg N/yr for past, present, and 2020 emissions, respectively.

Figure 10a shows monthly-mean time series of the mass of ozone in the 30°N-60°N free tropospheric control volume for the past, present, and future. The corresponding net chemical tendencies are provided in Figure 10b. From preindustrial to present, ozone mass in the winter increases by 25% and in the spring increases by 45%. These increases are primarily due to the dramatic shift in the net chemical tendency from strongly negative in preindustrial times to strongly positive in the present. The 2020 ozone level shows a further 15-20% increase in O_3 mass and is consistent with the even greater net chemical production. All three cases follow a similar seasonal cycle, with a winter-spring maximum and a fall minimum. However, the preindustrial maximum is transport-dominated and occurs in the late winter, while the present maximum is pushed into the spring due to a chemical net-production which is driven by the large increase in NO_x levels. Even greater 2020 emissions push the maximum into May. The effect of NO_x emissions on net chemistry for the zonal volume is also most pronounced in the springtime (see Figure 10b), where preindustrial chemistry destroys a net of 5-10 Tg O_3/month. Presently, springtime chemistry produces 3-5 Tg O_3/month, and that increases to 5-10 TgO_3/yr for 2020 NO_x emission levels. Similar results (winter to spring shift in the O_3 maximum) were recently reported for another GCTM ozone simulation [*Roelofs et al.*, 1997].

6. Uncertainty Discussion

Given that theoretical analysis and numerical simulation are the bases of this study, one should examine the observational

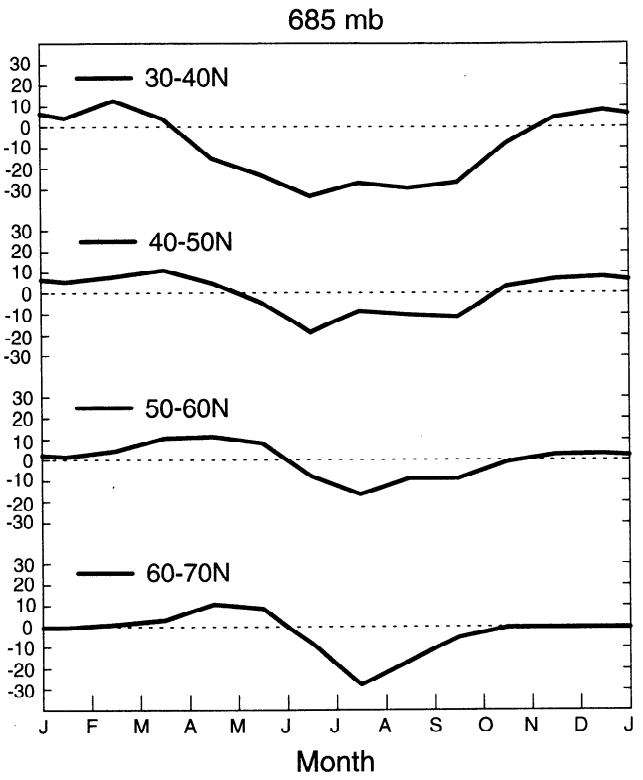

Figure 7. Annual time series of zonally averaged ozone photochemical tendency (ppbv O_3/month) for the 685-mbar level (~2-4 km) between 30°N and 70°N.

underpinnings. As previously discussed, our simulation of O_3 is in good agreement with ~90% of over 300 seasonal observations and in even better agreement with the subset of those data from the NH midlatitude free troposphere [*Levy et al.*, 1997; H. Levy et al., manuscript in preparation, 1998]. Our calculated ozone spring maximum for the zonal volume under study is consistent with the available observations from nonpolluted regions [*Logan*, 1985; *Oltmans et al.*, 1996; S. Oltmans, private communication, 1997]. The CH_4-CO-H_2O-NO_x chemical mechanism which dominates the chemical tendencies, and upon which the theory behind the seasonal shift in the "balance point" is based, is supported by an extensive array of laboratory kinetic studies. Moreover, our calculated chemical tendencies compare well with a number of analyses based on data from regional field experiments [e.g., *Chameides et al.*, 1992; *Klonecki and Levy*, 1997]. Finally, recent analyses of observations taken over the extratropical western North Pacific in February-March 1994 during the Pacific Exploratory Mission (PEM-West B) Campaign [*Crawford et al.*, 1997] are consistent with our primary conclusion of winter-spring net chemical production in the extratropical free troposphere and with our finding that the early spring net production drops sharply at higher latitudes, as we show in Figure 6.

In our calculations the balance point and the magnitude of net production depend critically on the levels of NO_x [*Klonecki and Levy*, 1997]. A recent extensive summary of most available observations through 1996 by *Emmons et al.* [1997] concluded that only an approximate global observed climatology was possible for NO_x, which varies by orders of magnitude between polluted and clean regions. They also concluded that the selection of models they examined, while showing significant disagreement among themselves, were consistent to 1 order of magnitude at all seasons and latitudes, though the GCTM's were not consistent as to whether NO_x increased or decreased in winter in the remote free troposphere. Another recent GCTM simulation [*Jaffe et al.*, 1997] finds midtropospheric NO_x too low to support net production in the winter and spring, while a second simulation with the same transport, but different chemistry and sources [*Kraus et al.*, 1996], appears to be in agreement with our analysis. While the *Emmons et al.* [1997] data set is an incomplete sample of the real world and there is clearly a need for seasonal observations of NO_x in the free troposphere, we do believe that their data set, when combined with recent new data, is sufficient to critically evaluate our GCTM simulation of NO_x. As reported in section 2, our NO_x fields are in reasonable agreement with the large majority of available observations and appear to be realistic.

While it is clear that the GCTM's simulation of NO_x is potentially the major source of uncertainty in this study, one should also note that the winter-spring ozone maximum is an extremely robust feature, with a tenfold increase in NO_x emissions only moving the maximum from February to April (see Figure 10). Moreover, while Figure 10 shows that the sign of the net chemical tendency term and its role in the winter-spring maximum changes for greatly reduced NO_x emissions, the winter-spring net chemical production only strengthens with a doubling of present estimated emissions. As a test of our conclusion's sensitivity to a possible high NO_x bias in our simulated NO_x fields, noting that no such bias was in fact found, we uniformly reduced all NO_x fields used in the O_3 simulation by 25% and still found a winter-spring maximum in the total mass of O_3 and net chemical production, though it does turn neutral 1 month earlier.

Furthermore, while uncertainties of 20-40 pptv in the monthly mean for the zonal slab under analysis can make the difference between net production and destruction when summer-fall turns to winter-spring, NO_x levels in the background troposphere are highly variable and are seldom represented by their mean values [*Moxim et al.*, 1996; *Ridley et al.*, 1997]. The elevated levels that dominate net chemical production of ozone are discrete events and may be less sensitive to uncertainties of 20-40 pptv than is the monthly mean.

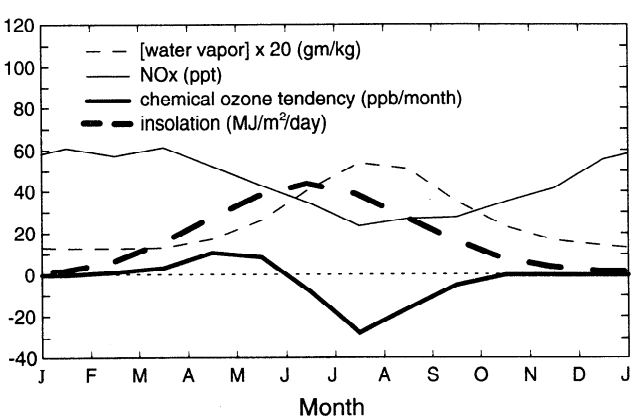

Figure 8. Annual time series of zonally averaged NO_x, water vapor, insolation, and photochemical ozone tendency for the 685-mbar level between 60°N and 70°N. Water vapor is multiplied by 20.

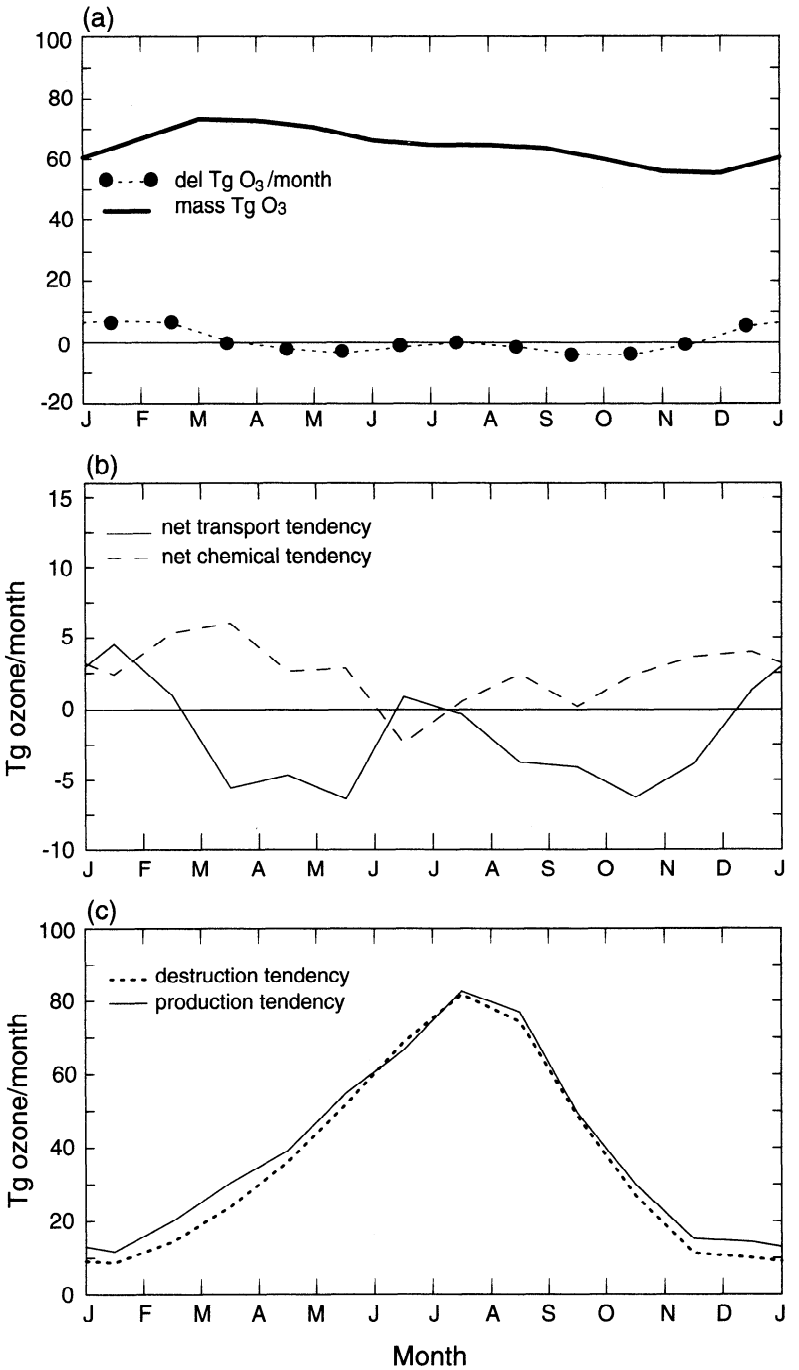

Figure 9. (a) Annual time series of simulated ozone mass (teragrams) and net tendency (chemical + transport) between 30° and 60°N for the free troposphere (~ 2-10 km). Figure 9b shows net transport and chemical tendencies, and Figure 9c shows chemical production and destruction tendencies. All tendency terms have units of Tg/month.

Another approximation, which may lead to an underestimation of spring ozone production, is our model's lack of nonmethane hydrocarbon chemistry. For example, ethane, propane, and acetone also accumulate in the free troposphere during winter [e.g., *Penkett et al.*, 1993]. Their presence during spring would increase the supply of peroxy radicals (HO_2 and RO_2) and amplify ozone production via (R5) and an analogue of (R6) [e.g., *Singh et al.*, 1995]. However, they are only expected to be significant in the upper troposphere, where H_2O concentrations are very low, and we have already shown O_3 to be relatively insensitive to enhanced production.

7. Conclusions

On the basis of our global simulation of tropospheric ozone and on our analysis of its seasonal behavior and photochemistry, we conclude the following for the NH midlatitude free

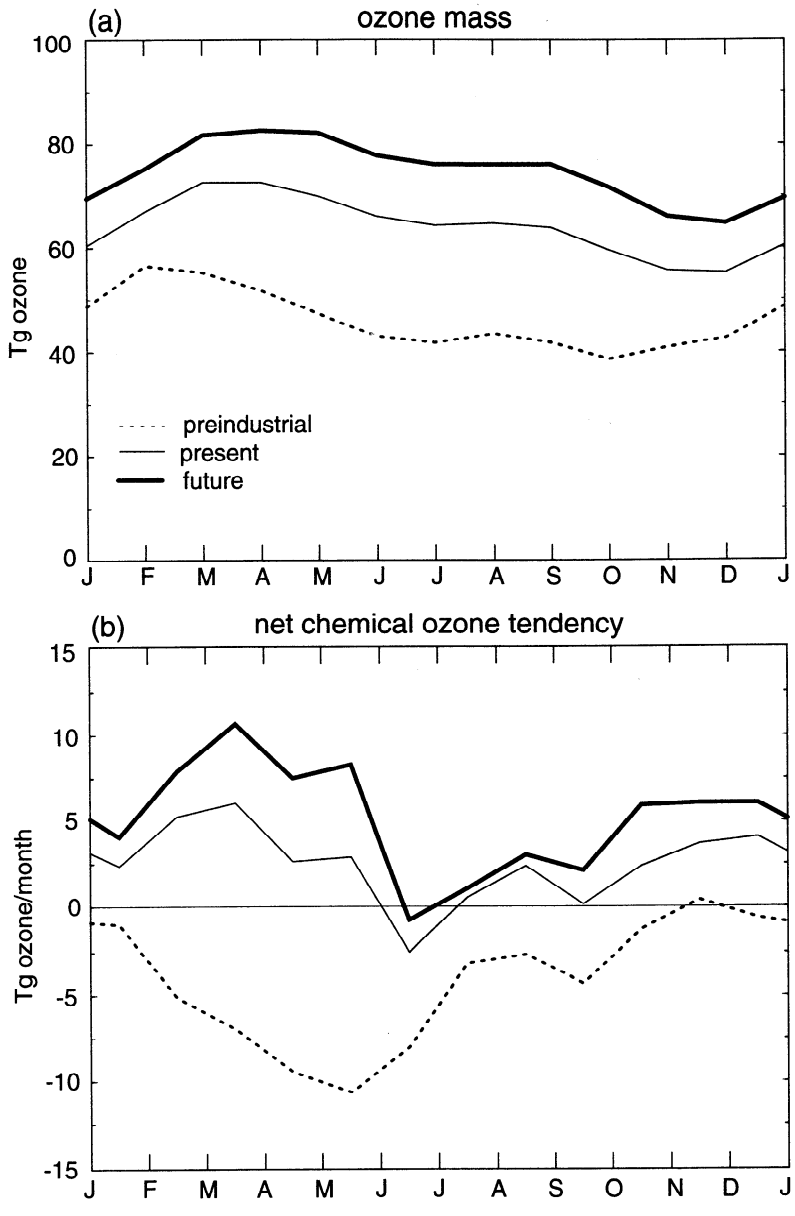

Figure 10. (a) Annual time series of past, present, and future (2020) simulated ozone mass (teragrams) between 30°N and 60°N for the free troposphere (~2-10 km). (b) Corresponding photochemical ozone tendencies (Tg/month) for each case.

troposphere, an area heavily influenced by both anthropogenic emissions and stratospheric-tropospheric exchange.

1. The seasonal behavior of the total mass of ozone in the volume, a winter-spring maximum and a late fall minimum, is a robust feature of this study stretching from our preindustrial simulation with a transport-dominated February maximum to the present March-April maximum with comparable contributions from transport and in situ chemistry. The maximum pushes further into April-May with projected 2020 NO_x emissions.

2. While the much stronger summer chemistry is essentially in balance, the relatively weak chemistry of the winter and early spring produces the net production that is a major component of the present and 2020 spring maxima.

3. Below 500 mbar, the atmosphere experiences a large-scale switch from chemical destruction of ozone in the summer to production in the winter and spring. Wintertime climatic conditions require less NO_x than in the summer to be net productive, and, in addition, NO_x levels rise in remote regions as surface pollution spreads farther from source regions. Net production maximizes for a brief period in early spring as insolation increases, a time when the atmosphere is still relatively dry and high winter NO_x levels have yet to be depleted by OH oxidation.

4. Human activity has increased the total ozone mass by ~20% in the winter and ~45% in the spring and has dramatically changed the role of in situ winter-spring chemistry from net destruction under preindustrial conditions to the present net production. Projected 2020 levels of NO_x emissions lead to even greater winter-spring net chemical production.

Acknowledgments. One of us (H.L.II) acknowledges earlier debates on this topic with S. C. Liu; we all thank M. J. Phadnis, C. Andronache, and J. D. Mahlman for their careful reading of the manuscript and for their helpful comments; and we acknowledge the thoughtful and helpful comments of two anonymous reviewers. One of us (J.J.Y.) acknowledges support from NASA grant NAG5-3855, and one of us (A.A.K.) acknowledges support from NASA grant NGT 5-30015.A01.

References

Benkovitz, C. M., M. T. Scholtz, J. Pacyna, L. Tarrasón, J. Dignon, E. C. Voldner, P. A. Spiro, J. A. Logan, and T. A. Graedel, Global gridded inventories of anthropogenic emissions of sulfur and nitrogen, *J. Geophys. Res., 101,* 29,239-29,253, 1996.

Bernsten, T. K., and I. S. A. Isaksen, A global three-dimensional chemical transport model for the troposphere, 1, Model description and CO and ozone results, *J. Geophys Res., 102,* 21,239-21,280, 1997.

Chameides, W. L., et al., Ozone precursor relationships in the ambient atmosphere, *J. Geophys. Res., 97,* 6037-6055, 1992.

Crawford J., et al., An assessment of ozone photochemistry in the extratropical western North Pacific: Impact of continental outflow during the late winter/early spring, *J. Geophys. Res., 102,* 28,469-28,487, 1997.

Emmons, L., et al., Climatologies of NO_x and NO_y: A comparison of data and models, *Atmos. Environ., 31,* 1851-1904, 1997.

Energy Information Administration, *International Energy Outlook 1997,* DOE/EIA-0484(97), Washington, D. C., 1996.

Follows, M. J., and J. F. Austin, A zonal average model of the stratospheric contributions to the tropospheric ozone budget, *J. Geophys. Res., 97,* 18,047-18,060, 1992.

Galloway, J. N., H. Levy II, and P. S. Kasibhatla, Year 2020: Consequences of population growth and development on deposition of oxidizes nitrogen, *Ambio, 23,* 120-123, 1994.

Hamilton, K. R., R. J. Wilson, J. D. Mahlman, and L. J. Umscheid, Climatology of the SKYHI troposphere-stratosphere-mesosphere general circulation model, *J. Atmos. Sci., 52,* 5-43, 1995.

Jacob, D. J., J. A. Logan, G. M. Gardner, R. M Yevich, C. M. Spivakovsky, and S. C. Wofsy, Factors regulating ozone over the United States and its export to the global atmosphere, *J. Geophys. Res., 98,* 14,817-14,826, 1993.

Jaffe, D. A., T. K. Bernsten, and I. S. A. Isaksen, A global three-dimensional chemical transport model, 2, Nitrogen oxides and nonmethane hydrocarbon results, *J. Geophys. Res., 102,* 21,281-21,296, 1997.

Kasibhatla, P. S., H. Levy II, and W. J. Moxim, Global NO_x, HNO_3, PAN and NO distributions from fossil-fuel combustion emissions: A model study, *J. Geophys. Res., 98,* 7165-7180, 1993.

Kasibhatla, P. S., H. Levy II, A. A. Klonecki, and W. L. Chameides, Three-dimensional view of the large-scale tropospheric ozone distribution over the North Atlantic Ocean during summer, *J. Geophys. Res., 101,* 29,305-29,316, 1996.

Klonecki, A. A., Model study of the tropospheric chemistry of ozone, Ph.D. thesis, Princeton Univ., Princeton, N. J., 1998.

Klonecki, A. A., and H. Levy II, Tropospheric chemical ozone tendencies in $CO\text{-}CH_4\text{-}NO_y\text{-}H_2O$ system: Their sensitivity to variations in environmental parameters and their application to a global chemistry transport model study, *J. Geophys. Res., 102,* 21,221-21,237, 1997.

Kraus, A. B., F. Rohrer, E. S. Grobler, and D. H. Ehhalt, The global tropospheric distribution of NO_x by a three-dimensional chemical tracer model, *J. Geophys. Res., 101,* 18,587-18,604, 1996.

Levy, H., II, Normal atmosphere: Large radical and formaldehyde concentrations predicted, *Science, 173,* 141-143, 1971.

Levy, H., II, J. D. Mahlman, and W. J. Moxim, Tropospheric ozone: The role of transport, *J. Geophys. Res., 90,* 3753-3772, 1985.

Levy, H., II, W. J. Moxim, and P. S. Kasibhatla, A global three-dimensional time-dependent lightning source of tropospheric NO_x, *J. Geophys. Res., 101,* 22,911-22,922, 1996.

Levy, H., II, P. S. Kasibhatla, W. J. Moxim, A. A. Klonecki, A. I. Hirsch, S. J. Oltmans, and W. L. Chameides, The global impact of human activity on tropospheric ozone, *Geophys. Res. Lett., 24,* 791-794, 1997.

Lin, X. M., and S. C. Liu, On the nonlinearity of tropospheric ozone production, *J. Geophys. Res., 93,* 15,879-15,888, 1988.

Liu, S. C., M. Trainer, F. C. Fehsenfeld, D. D. Parrish, E. J. Williams, D. W. Fahey, G. Hubler, and P. C. Murphy, Ozone production in the rural troposphere and the implications for regional and global ozone distributions, *J. Geophys. Res., 92,* 4191-4207, 1987.

Logan, J. A., Tropospheric ozone: Seasonal behavior, trends, and anthropogenic influence, *J. Geophys. Res., 90,* 10,463-10,482, 1985.

Mahlman, J.D., Long-term dependence of surface fallout fluctuations upon tropopause cyclogenesis, *Arch. Meteorol. Geophys. Bioklimatol., Ser. A, 18,* 299-311, 1969.

Mahlman, J. D., and W. J. Moxim, Tracer simulation using a global general circulation model: Results from a midlatitude instantaneous source experiment, *J. Atmos. Sci., 35,* 1340 - 1374, 1978.

Mahlman, J. D., H. Levy II, and W. J. Moxim, Three-dimensional tracer structure and behavior as simulated in two ozone precursor experiments, *J. Atmos. Sci., 37,* 655-685, 1980.

Moody, J., S. J. Oltmans, H. Levy II, and J. T. Merrill, Transport climatology of tropospheric ozone: Bermuda, 1988-1991, *J. Geophys. Res., 100,* 7179-7194, 1995.

Moxim, W. J., H. Levy II, and P. S. Kasibhatla, Simulated global tropospheric PAN: Its transport and impact on NO_x, *J. Geophys. Res., 101,* 12,621-12,638, 1996.

Muller, J.-F., and G. Brasseur, IMAGES: A three-dimensional chemical transport model of the global troposphere, *J. Geophys. Res., 100,* 16,445-16,490, 1995.

Oltmans, S. J., Surface ozone measurements in clean air, *J. Geophys. Res., 86,* 1174-1180, 1981.

Oltmans, S. J., and H. Levy II, Seasonal cycle of surface ozone over the western North Atlantic, *Nature, 358,* 392-394, 1992.

Oltmans, S.J., and H. Levy II, Surface ozone measurements from a global network, *Atmos. Environ., 23,* 9-24, 1994.

Oltmans, S. J., D. J. Hofmann, J. A. Lathrop, J. M. Harris, W. D. Komhyr, and D. Kuniyuki, Tropospheric ozone during Mauna Loa Observatory Photochemistry Experiment 2 compared to long-term measurements from surface and ozonesonde observations, *J. Geophys. Res., 101,* 14,569-14,580, 1996.

Oort, A. H., Global atmospheric circulation statistics, 1958-1973, *NOAA Prof. Pap. 14,* 180 pp., U.S. Gov. Print. Off., Washington, D. C., 1983.

Parrish, D. D., J. S. Holloway, M. Trainer, P. C. Murphy, G. L. Forbes, and F. C. Fehsenfeld, Export of North American ozone pollution to the North Atlantic Ocean, *Science, 259,* 1436-1439 1993.

Penkett, S. A., and K. A. Brice, The spring maximum in photochemical oxidants in the northern hemisphere, *Nature, 319,* 655-657, 1986.

Penkett, S. A., N. J. Blake, P. Lightman, A. R. W. Marsh, P. Anwyl, and G. Butcher, The seasonal variation of nonmethane hydrocarbons in the free troposphere over the North Atlantic Ocean: Possible evidence for extensive reaction of hydrocarbons with the nitrate radical, *J. Geophys. Res., 98,* 2865-2885, 1993.

Penkett, S. A., C. E. Reeves, B. J. Brandy, J. M. Kent, and H. R. Richer, Comparison of calculated and measured peroxide data collected in marine air to investigate prominent features of the annual cycle of ozone in the troposphere, *J. Geophys. Res., 103,* 13,377-13,388, 1998.

Ridley, B. A., E. L. Atlas, J. G. Walega, G. L. Kok, T. A. Staffelbach, J. P. Greenberg, F. E. Grahek, P. G. Hess, and D. D. Montzka, Aircraft measurements made during the spring maximum of ozone over Hawaii: Peroxides, CO, O_3, NO_y, condensation nuclei, selected hydrocarbons, halocarbons, and alkyl nitrates between 0.5 and 9 km altitude, *J. Geophys. Res., 102,* 18,935-18,961, 1997.

Roelofs, G.-J., and J. Lelieveld, Model study of the influence of cross-tropopause O_3 transports on tropospheric O_3 levels, *Tellus, Ser. B, 49,* 38-55, 1997.

Roelofs, G.-J., J. Lelieveld, and R. van Dorland, A three-dimensional chemistry/general circulation model simulation of anthro-

pogenically derived ozone in the troposphere and its radiative climate forcing, *J. Geophys. Res.*, *102*, 23,389-23,401, 1997.

Singh, H. B., M. Kanakidou, P. J. Crutzen, and D. J. Jacob, High concentrations and chemical fate of oxygenated hydrocarbons in the global atmosphere, *Nature, 378*, 50-54, 1995.

Soden, B. J., and F. P. Bretherton, Interpretation of TOVS water vapor radiances in terms of layer-average relative humidities: Method and climatology for the upper, middle, and lower troposphere, *J. Geophys. Res.*, *101*, 9,333-9,343, 1996.

van Aardenne, J. A., G. R. Carmichael, H. Levy II, D. Streets, and L. Hordijk, Anthropogenic NO_x emissions in Asia in the period 1990 to 2020, *Atmos. Environ.*, in press, 1998.

Yienger, J. J., and H. Levy II, Empirical model of global soil-biogenic NO_x emissions, *J. Geophys. Res.*, *100*, 11,447-11,464, 1995.

G. R. Carmichael and J. J. Yienger, Center for Global and Regional Environmental Research, University of Iowa, Iowa City, IA 52242. (e-mail: gcarmich@icaen.uiowa.edu; jyienger@cgrer.uiowa.edu)

A. A. Klonecki, Atmospheric and Oceanic Sciences Program, Princeton University, Princeton, NJ 08542. (e-mail: aak@gfdl.gov)

H. Levy II and W. J. Moxim, NOAA Geophysical Fluid Dynamics Laboratory, Princeton, NJ 08542. (e-mail: hl@gfdl.gov; wm@gfdl.gov)

(Received February 12, 1998; revised September 28, 1998; accepted September 30, 1998.)